Renewable Energy 224 (2024) 120193

Contents lists available at ScienceDirect

Renewable Energy

journal homepage: www.elsevier.com/locate/renene

Performance analysis of a novel thermoelectric-based battery thermal management system

Ding Luo [a,b,***], Ye Zhao [a], Jin Cao [a], Wei-Hsin Chen [d,e,f], Yulong Zhao [c,**], Bingyang Cao [b,*]

[a] College of Electrical Engineering & New Energy, China Three Gorges University, Yichang, 443000, China
[b] Key Laboratory for Thermal Science and Power Engineering of Ministry of Education, Department of Engineering Mechanics, Tsinghua University, Beijing, 100084, China
[c] Hebei Key Laboratory of Thermal Science and Energy Clean Utilization, Hebei University of Technology, Tianjin, 300401, China
[d] Department of Aeronautics and Astronautics, National Cheng Kung University, Tainan, 701, Taiwan
[e] Research Center for Smart Sustainable Circular Economy, Tunghai University, Taichung, 407, Taiwan
[f] Department of Mechanical Engineering, National Chin-Yi University of Technology, Taichung, 411, Taiwan

ARTICLE INFO

Keywords:
Thermoelectric cooling
Battery thermal management
Air cooling
Water cooling
Thermal behavior

ABSTRACT

To ensure the optimal operating temperature of lithium-ion batteries, a novel thermoelectric-based battery thermal management system coupled with water cooling and air cooling is proposed in this work. Also, a hydraulic-thermal-electric multiphysics model is established to assess the system's thermal behavior. Through numerical simulations, the effect of different cooling parameters, including TEC (thermoelectric cooler) input current, air convection heat transfer coefficient, and cooling water flow rate on thermal performance is comprehensively analyzed. The results show that the introduction of thermoelectric cooling into battery thermal management can amplify the cooling ability of traditional air cooling and water cooling, and the cooling power and COP (coefficient of performance) of thermoelectric coolers first increase and then decrease with the increase of input current. Under the air convection heat transfer coefficient of 50 W m^{-2} K^{-1}, water flow rate of 0.11 m/s, and TEC input current of 5 A, the battery thermal management system reaches the optimal thermal performance, corresponding to the maximum temperature and temperature difference of 302.27 K and 3.63 K respectively. However, the cooling parameters of these three factors interact with each other, and it is vital to select appropriate cooling parameters to balance the thermal performance and energy consumption of the battery thermal management system. More importantly, this work provides a brand-new idea for the thermal management of batteries.

1. Introduction

Due to the utilization of fossil fuels in the industry, issues such as the energy crisis, environmental pollution, and global warming have gradually escalated, leading to the transition from fuel-powered conventional system to zero-emission or hybrid electric system [1]. Governments have announced plans for the future of the automotive industry, to phase out conventional gasoline vehicles and encourage the development of electric and hybrid vehicles [2–4]. Compared with traditional vehicles, electric ones have gradually been recognized for their advantages of low energy consumption, environmental friendliness, and reliability. In particular, the lithium-ion battery-based vehicle has become a widely adopted technological option, primarily owing to its high energy density and long life [5,6]. On one hand, lithium-ion batteries generally operate within the temperature range of −20 °C–60 °C [7], but the heat generated during charging or discharging can cause the temperature to increase, resulting in overheating or even thermal runaway. On the other hand, operating the battery below 0 °C hampers charge transfer kinetics, leading to reduced electrolyte conductivity and slower diffusion of solid lithium. To preserve the normal temperature working range of Lithium-ion batteries, the implementation of a battery thermal management system (BTMS) is imperative.

The current technical routes of the BTMS mainly include heat pipe,

* Corresponding author.
** Corresponding author.
*** Corresponding author. College of Electrical Engineering & New Energy, China Three Gorges University, Yichang, 443000, China.
E-mail addresses: Ding_L@outlook.com (D. Luo), 202208580121346@ctgu.edu.cn (Y. Zhao), caojin@ctgu.edu.cn (J. Cao), weihsinchen@gmail.com (W.-H. Chen), zhaoyulong@hebut.edu.cn (Y. Zhao), caoby@tsinghua.edu.cn (B. Cao).

https://doi.org/10.1016/j.renene.2024.120193
Received 9 August 2023; Received in revised form 4 January 2024; Accepted 19 February 2024
Available online 20 February 2024

Nomenclature

Symbols

A	area, m^2
Cp	specific heat, $J{\cdot}kg^{-1}{\cdot}K^{-1}$
$\vec{E}$	electric field density vector, $V{\cdot}m^{-2}$
h	heat transfer coefficient, $W{\cdot}m^{-1}{\cdot}K^{-1}$
I	current, A
$\vec{J}$	current density vector, $A{\cdot}m^{-2}$
k	thermal conductivity, $W{\cdot}m^{-1}{\cdot}K^{-1}$
l	thermoelectric semiconductor height, m
N	number of thermoelectric couples
p	pressure, Pa
P	input power of TEC, W
Q	heat generation, W
R	resistance, Ω
T	temperature, K
$\vec{v}$	velocity vector, m/s
v	absolute velocity, m/s

Greek symbols

α	Seebeck coefficient, $\mu V{\cdot}K^{-1}$
σ	electrical conductivity, $S{\cdot}m^{-1}$
ρ	density, $kg{\cdot}m^{-3}$
μ	dynamic viscosity, Pa·s
φ	electrical potential, V

Subscripts

air	air
ce	ceramic plates
co	copper electrodes
C	cold end
g	heat generation
H	hot end
m	material
n	n-type thermoelectric semiconductors
p	p-type thermoelectric semiconductors
pn	the junction Seebeck coefficient
s	energy source term
to	total resistance of TEC
tec	thermoelectric coolers
w	water

Abbreviations

BTMS	battery thermal management systems
CFD	computational fluid dynamics
TEC	thermoelectric coolers

phase change, air cooling, water cooling, and thermoelectric cooling-based thermal management techniques. Among these, air cooling and liquid cooling-based BTMS are preferred for their simplicity and affordability, making them widely adopted. However, the temperature uniformity of batteries is hard to be accurately adjusted. Researchers have carried out many studies to address this issue. Kirad et al. [8] investigated the relationship between battery spacing and cooling efficiency, airflow velocity, and discharge rate; Their results demonstrate that cooling efficiency is notably impacted by the transverse spacing, temperature uniformity, and longitudinal spacing between cells. Fan et al. [9] studied the air cooling performance with different battery pack arrangements, including aligned, interleaved, and crossed structures; Based on their findings, it was concluded that the aligned arrangement delivers optimal cooling performance and temperature uniformity. Li et al. [10] proposed a multi-objective optimization method to design an efficient air-cooled system; Through comparison, the optimized system outperformed the traditional structure. Liquid cooling, in comparison to air cooling, proved to be more efficient and extensively employed. The cooling efficiency of liquid cooling-based BTMS has been the subject of numerous investigations, which have primarily focused on streamlining flow channel structures and employing efficient working fluids and compact channels. Menale et al. [11] tested the cooling performance of the BTMS with different heat transfer fluids; The experimental results indicated that the perfluoropolyether liquid can maintain the optimal temperature range of batteries under harsh conditions. Zhou et al. [12] developed a half-helix duct-based liquid cooling BTMS, which outperformed the traditional jacket-based BTMS due to the small fluid volume and no stagnant zone. Panchal et al. [13] designed a water cooling-based BTMS using a microchannel cold plat and studied its cooling performance through computational fluid dynamics (CFD) methods. Du et al. [14] analyzed the effect of different cooling plate parameters on the cooling performance of $LiFePO_4$ bag battery packs; They found that the battery charging process is significantly affected by the inlet flow rate and the size of the cooling channel. However, it is difficult to adjust the thermal uniformity of the battery both for the liquid cooling-based or air cooling-based BTMS.

To achieve that each battery cell operates at almost the same operating temperature, researchers [15,16] proposed several new BTMS. The heat pipe-based BTMS is a good candidate for achieving high temperature uniformity among numerous battery cells by utilizing the isothermal heat transfer characteristics of heat pipes. Chavan et al. [15] proposed a cylindrical BTMS that utilizes both heat pipe and liquid cooling methods, which includes two heat dissipation systems: an active one (cold plate) and a passive one (heat pipe); The results demonstrated notable improvements in both cooling performance and the uniformity of battery temperature. Ren et al. [16] designed an air cooling-based BTMS combined with an array of U-shaped micro-heat pipes; Through the comparison of three cooling methods, including passive air cooling with U-shaped heat pipes, passive air cooling without U-shaped heat pipes, and active air cooling with U-shaped heat pipes, the researchers found that the active air cooling with U-shaped heat pipes was able to effectively manage the increase in battery temperature while ensuring a homogeneous temperature profile across the battery. However, the structural configuration of heat pipes poses challenges in adapting to different battery shapes, limiting their widespread application in BTMS. Another effective way to enhance the temperature uniformity of battery cells is to apply phase change materials in the BTMS, where the battery temperature is adjusted by utilizing the latent heat released or absorbed by solid-liquid phase change materials during the curing or liquefaction process. Ling et al. [17] presented a hybrid thermal management system that utilizes both forced air cooling and phase change materials for effective temperature control in lithium-ion batteries; The results demonstrated that the system, when coupled with forced air cooling, efficiently controlled the battery pack's maximum temperature below 50 °C, exhibiting a temperature difference of less than 3 °C. This approach offers advantages such as a simple structure, excellent temperature uniformity, and no extra energy consumption. Nonetheless, the heat dissipation performance of phase change materials is compromised by their inadequate thermal conductivity [18], rendering them unsuitable for high thermal production conditions encountered in batteries. To solve this problem, high thermal conductivity substances are added to the phase change material to improve its thermal conductivity, such as metal foam [19–21], carbon fiber [22,23], graphite [24], and so on. In addition, the addition of fins is also a good approach to solving the limited thermal conductivity of phase change materials [25].

Thermoelectric refrigeration is a solid-state refrigeration technology

that uses electrical energy directly through the Peltier effect to achieve cooling, with the advantages of arbitrary size scaling, no vibration, high reliability, and high-temperature control accuracy. As a new type of BTMS, the thermoelectric-based BTMS has gradually attracted wide attention in recent years because of its advantages of precise temperature control and fast temperature response speed. In a previous work [26], published in 'Nature Energy', the authors pointed out that the BTMS encounters a fundamental challenge of conflicting demands under high- and low-temperature environments. At high temperatures, efficient heat transfer is required to reduce the battery temperature, however, at low temperatures, efficient thermal insulation is required to maintain the heat generated inside the battery. In this context, existing thermal management routes based on water cooling, air cooling, phase change materials, and heat pipe can not meet the above requirements, while the thermoelectric-based BTMS can effectively address this challenge. Song et al. [27] developed a new BTMS for base station backup batteries, which combines thermoelectric devices and phase change materials; Through theoretical analysis, it has been proved that the coupling of thermoelectric devices and phase change materials can effectively improve the temperature uniformity and prolong the thermal insulation process. Furthermore, Liu et al. [28] utilized fins to enhance the performance of the BTMS coupled with thermoelectric devices and phase change materials, and studied the influence of fin thicknesses on thermal performance; They found that the temperature control time exhibits a 12% extension with the increase of fins from 2 mm to 8 mm, but at the same time, the temperature difference increased by 13.7%. However, the current performance investigation on the thermoelectric-based BTMS mainly depends on CFD simulations or simple analysis, lacking systematic analysis of its performance, without considering the multiphysics coupling characteristics. There is a lack of accurate and systematic performance analysis about the thermoelectric-based BTMS.

By combining the working characteristics between traditional air/water cooling methods and thermoelectric refrigeration, this article proposes a novel thermoelectric-based BTMS with an inner and outer double-layer TEC structure to ensure the optimal temperature working environment of the battery. In the proposed system, the use of TECs can enhance the cooling capacity of air/water cooling, while conversely, air/water cooling can ensure a low temperature differential for TECs. Besides, a fluid-thermal-electric multi-physical field coupling model is established to systematically analyze the thermal behavior of the thermoelectric-based BTMS under different parameters. This paper is structured as follows: the first section provides an overview of recent advancements in battery thermal management; The second section introduces the structure of the proposed BTMS; The third section gives a detailed introduction of the multiphysics model; The fourth section conducts a thermal performance analysis of the system under different operating conditions; Finally, the key findings are summarized in the last section.

2. Structure of the thermoelectric-based battery thermal management system

The proposed novel thermoelectric-based BTMS consists of five parts: four heat sinks, 12 thermoelectric coolers (TECs), a honeycomb framework, 12 $LiFePO_4$ battery cells, and a water channel, as shown in Fig. 1. To effectively dissipate the heat on the hot side of TECs and reduce weight, the heat sink is made of aluminum materials, and each heat sink features 40 fins with a height of 4 mm and a thickness of 1 mm. The TEC is composed of 127 pairs of thermoelectric semiconductors (1.4 mm × 1.4 mm × 1.6 mm), 256 copper electrodes (3.8 mm × 1.4 mm × 0.4 mm), and two ceramic plates (40 mm × 40 mm × 0.7 mm), where thermoelectric semiconductors are connected in series by copper electrodes and sandwiched between two ceramic plates. Eight TECs are distributed on the outer side of the framework, while four TECs are distributed on the inner side. When the current passes through the TEC, the side where carriers accumulate will release heat (hot side), whereas another side will absorb heat (cold side), and the cold side of TECs is close to the battery cell. The aluminum honeycomb framework is designed with 12 holes to place battery cells. The $LiFePO_4$ battery cell is designed with a height of 50 mm and a diameter of 16 mm. During the discharging process, the battery cell will generate tremendous heat, which is absorbed by both inner and outer TECs. In consideration of the space limitations inside the aluminum framework, a water channel with a diameter of 25 mm is adopted to ensure heat dissipation capacity. The structural design with internal water cooling and external air cooling helps to reduce the temperature difference of battery cells, while the TEC, as a temperature controller, is conducive to achieving precise temperature control. Detailed material properties of the thermoelectric-based BTMS are given in Table 1, in which the thermoelectric material

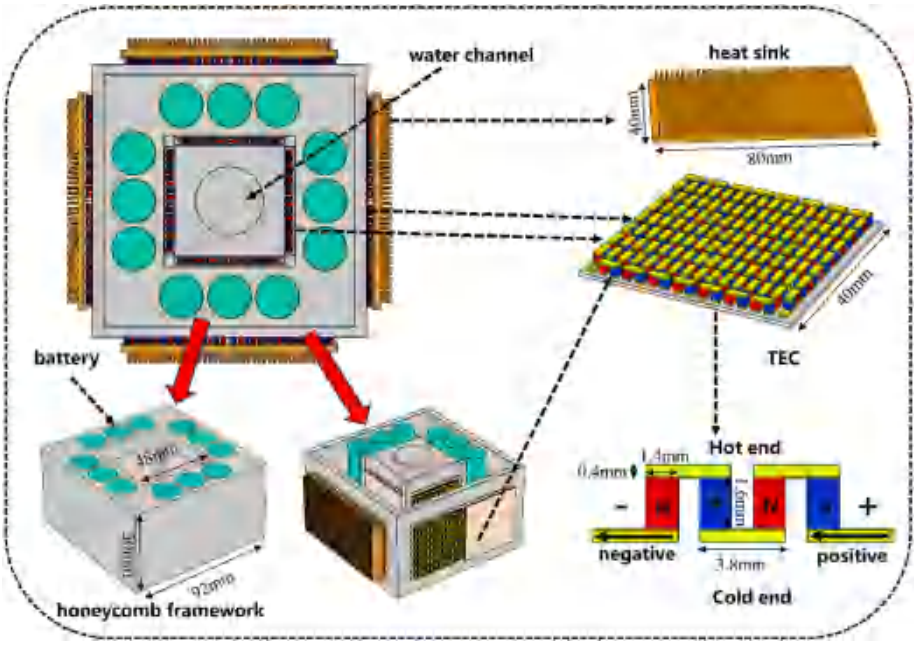

Fig. 1. Architecture of the novel thermoelectric-based BTMS.

Table 1
Material properties of the thermoelectric-based BTMS.

Component	Material name	Seebeck coefficient($\mu V \cdot K^{-1}$)	Thermal conductivity($W \cdot m^{-1} \cdot K^{-1}$)	Electrical conductivity($S \cdot m^{-1}$)
heat sink and framework	aluminum	–	238	–
battery cell	$LiFePO_4$	–	x:y:z = 15.3:15.3:0.9	–
ceramic plate	ceramic	–	22	–
p-type semiconductors	p-type Bi_2Te_3 materials	$-1.593 \times 10^{-9}T^2 + 1.364 \times 10^{-6}T - 7.062 \times 10^{-5}$	$1.071 \times 10^{-5}T^2 - 8.295 \times 10^{-3}T + 2.625$	$1.311T^2 - 1.364 \times 10^3T + 4.023 \times 10^5$
n-type semiconductors	n-type Bi_2Te_3 materials	$7.393 \times 10^{-11}T^2 - 2.500 \times 10^{-7}T - 8.494 \times 10^{-5}$	$1.870 \times 10^{-5}T^2 - 1.447 \times 10^{-2}T + 3.680$	$0.657T^2 - 7.136 \times 10^2T + 2.463 \times 10^5$
copper electrodes	copper		400	5.998×10^7

properties are provided by Hu et al. [29], and the thermal conductivity of batteries is anisotropic.

3. The hydraulic-thermal-electric multiphysics model

In the traditional BTMS, its thermal performance can be obtained by CFD simulations. However, the thermoelectric-based BTMS involves complex multiphysics coupling phenomena, and the CFD model can not meet the requirements of thermal prediction. For the purpose of ensuring the accuracy of numerical simulations, it is necessary to develop a multiphysics model under the consideration of coupling characteristics among different physical fields, including fluid flow, heat transfer, and thermoelectric conversion.

3.1. Basic equations

In the thermoelectric-based BTMS, different components follow different governing equations. For battery cells, the heat generation can be expressed as [30,31]:

$$Q_g = \frac{Q}{V} \tag{1}$$

where Q_g is the heat generation per unit volume. Q represents the total heat production power of 7.48 W. V represents the volume of a battery cell.

For cooling water, the hydraulic field can be described by the CFD theory. Besides, through a simple calculation, the Reynold number of the water flow is lower than 2300, and thus a laminar model is selected to simulate the fluid flow. Transport equations for the hydraulic field include [32]:

$$\nabla \cdot (\rho_w \vec{v}) = 0 \tag{2}$$

$$\nabla \cdot (\rho_w \vec{v}\vec{v}) = -\nabla p + \nabla[\mu(\nabla \vec{v} + \nabla \vec{v}^T)] \tag{3}$$

$$\nabla \cdot (\rho_w Cp_w \vec{v} T_w) - \nabla \cdot (k_w \nabla T_w) = 0 \tag{4}$$

where, ρ_w, $\vec{v}$, Cp_w, μ, p, k_w and T_w are the density, velocity vector, specific heat capacity, dynamic viscosity, pressure, thermal conductivity, and temperature of cooling water, respectively.

For the solid regions, the governing equation of the thermal field can be expressed by the energy conservation:

$$\nabla \cdot (k_m \nabla T) + Q_s = 0 \tag{5}$$

where, k_m represents the material thermal conductivity, and Q_s is the energy source term. In different components, Q_s can be written as:

$$Q_s = \begin{cases} Q_g & ; \text{battery cells} \\ \dfrac{\vec{J}^2}{\sigma_p} - \nabla\alpha_p(T)\vec{J}T_p - \dfrac{\partial\alpha_p(T)}{\partial T_p}T_p\vec{J}\cdot\nabla T & ; \text{p} - \text{type thermoelectric semiconductors} \\ \dfrac{\vec{J}^2}{\sigma_n} - \nabla\alpha_n(T)\vec{J}T_n - \dfrac{\partial\alpha_n(T)}{\partial T_n}T_n\vec{J}\cdot\nabla T & ; \text{n} - \text{type thermoelectric semiconductors} \\ \dfrac{\vec{J}^2}{\sigma_{co}} & ; \text{copper electrodes} \\ 0 & ; \text{heat sink, framework, and ceramic plates} \end{cases} \tag{6}$$

where α and σ are the Seebeck coefficient and the electrical conductivity of thermoelectric materials respectively. $\vec{J}$ is the current density vector. Subscripts p, n, and co represent p-type thermoelectric semiconductors, n-type thermoelectric semiconductors, and copper electrodes, respectively.

The components involved in current flow also follow governing equations of the electric field, which can be described by Ref. [33]:

$$\vec{J} = \sigma_m \vec{E} \tag{7}$$

$$\vec{E} = -\nabla\varphi + \alpha_{p/n}(T)\nabla T \tag{8}$$

$$\nabla \cdot \vec{J} = 0 \tag{9}$$

where φ and $\vec{E}$ represent the electric potential and the electric field density vector, respectively.

The hydraulic-thermal-electric multiphysics model could be characterized by Eqs (1)–(9). When combined with suitable boundary conditions, the model is able to be computed using numerical discretization methods. The numerical simulations in this work are carried out using the finite element method on the COMSOL platform.

3.2. Boundary conditions

This work primarily aims to study the thermal behavior of the novel thermoelectric-based BTMS under various operating conditions, including the convective heat transfer coefficient of cooling air, the flow speed of cooling water, and the TEC input current. The convective heat

transfer coefficient is defined on the contact surfaces between the heat sink and surroundings, which can be described by the following boundary condition:

$$-k\frac{\partial T}{\partial n}=h_{\mathrm{air}}(T_{\mathrm{air}}-T) \tag{10}$$

where, h_{air} is the convective heat transfer coefficient of cooling air, and $T_{\mathrm{air}}=293.15$ K is the air temperature. The value of h_{air} is referred from Ref. [34], with a range from 10 to 90 W m^{-2} K^{-1}.

For the flow speed of cooling water, the inlet velocity boundary condition is defined on the inlet surface of the water channel, and the water temperature is set as 293.15 K. The flow rate of the cooling water is set to vary from 0 to 0.5 m s^{-1}.

Besides, a current input boundary condition is defined on the positive pole of TECs, while the negative pole is set to be grounded. Considering that the cooling performance of the TEC is sensitive to its current input, the influence of current input on the thermal behavior of the BTMS is comprehensively investigated in the following sections.

3.3. Parameter definition

For the BTMS, maximum temperature ($T_{\max}$) and temperature difference (ΔT) are two key indexes to evaluate its thermal performance. Herein, $T_{\max}$ is defined as the maximum temperature of all battery cells, and ΔT is calculated as the temperature difference between the highest and lowest temperatures among all battery cells.

Besides, cooling power (Q_{C}) and coefficient of performance (COP) are two key indexes to estimate the cooling performance of the TEC, so as to study the application potential of the TEC in the field of thermal management. Q_{C} is determined by the heat absorption on the cold side of the TEC [35], which can be expressed as:

$$Q_{\mathrm{C}}=N\alpha_{\mathrm{pn}}IT_{\mathrm{C}}-\frac{1}{2}I^2R_{\mathrm{to}}-k_{tec}\Delta T \tag{11}$$

with

$$\alpha_{\mathrm{pn}}=\alpha_{\mathrm{p}}-\alpha_{\mathrm{n}} \tag{12}$$

$$k_{tec}=N\left(k_{\mathrm{p}}+k_{\mathrm{n}}\right)\frac{A_{\mathrm{p/n}}}{l_{\mathrm{p/n}}}+256k_{\mathrm{co}}\frac{A_{\mathrm{co}}}{l_{\mathrm{co}}}+2k_{\mathrm{ce}}\frac{A_{\mathrm{ce}}}{l_{\mathrm{ce}}} \tag{13}$$

$$R_{\mathrm{to}}=N\left(\frac{1}{\sigma_{\mathrm{p}}}+\frac{1}{\sigma_{\mathrm{n}}}\right)\frac{l_{\mathrm{p/n}}}{A_{\mathrm{p/n}}} \tag{14}$$

where, α_{pn} is the Seebeck coefficient of the thermoelectric couple, I represents the current passing through the TEC, R_{to} represents the total electrical resistance of thermoelectric semiconductors, k_{tec} represents the thermal conduction of the whole TEC, and $\Delta T = T_{\mathrm{H}}$ - T_{C} represents the temperature difference between the hot-side temperature (T_{H}) and the cold-side one (T_{C}) of the TEC.

In the case of active cooling, the heat of the TEC is released on its hot side, which can be expressed as:

$$Q_{\mathrm{H}}=N\alpha_{\mathrm{pn}}IT_{\mathrm{H}}+\frac{1}{2}I^2R_{\mathrm{to}}-k_{\mathrm{tec}}\Delta T \tag{15}$$

Therefore, the input power of the TEC can be obtained by:

$$P=Q_{\mathrm{H}}-Q_{\mathrm{C}}=I^2R_{\mathrm{to}}+N\alpha_{\mathrm{pn}}I\Delta T \tag{16}$$

Then, the COP is defined as the ratio of heat absorbed by the cold side of the TEC to the input power, which can be given by:

$$\mathrm{COP}=\frac{Q_{\mathrm{C}}}{P}=\frac{N\alpha_{\mathrm{pn}}IT_{\mathrm{C}}-\frac{1}{2}I^2R_{\mathrm{to}}-k_{\mathrm{tec}}\Delta T}{I^2R_{\mathrm{to}}+N\alpha_{\mathrm{pn}}I\Delta T} \tag{17}$$

3.4. Grid independence analysis

Excessive grid size can lead to substantial computational time savings but at the cost of sacrificing model accuracy, and conversely, reducing the grid size can improve accuracy but increase computational time. Therefore, it is crucial to select a reasonable grid size before conducting simulations in order to strike a balance between accuracy and computational time. To investigate the impact of grid parameters on the thermal performance of the BTMS, simulations are conducted using three different grid systems: Grid I, Grid II, and Grid III with 171023, 229532, and 328082 grids. The maximum temperatures ($T_{\max}$) for Grid I, Grid II, and Grid III are 308.64 K, 310.11 K, and 310.18 K, respectively. As the number of grids increases, the grid uncertainty gradually decreases. The relative uncertainty between Grid II and Grid III is decreased to within 0.07 K. As a result, all subsequent simulations are carried out using Grid II. The detailed configuration of Grid II for the BTMS is shown in Fig. 2.

3.5. Model validation

While the BTMS prototype is currently in the process of being manufactured, it is expected to be a time-consuming endeavor. Consequently, we adopt the experimental data from the previously published literature to validate the model in this work. The structure of the BTMS that combines TECs and heat pipes in Ref. [36] is built and numerically simulated using the developed steady-state hydraulic-thermal-electric multiphysics model. Fig. 3 illustrates the comparison of the maximum temperature difference between the experimental data in Ref. [36] and the simulation results in this work. Notably, the simulation results closely match the experimental data, exhibiting a maximum error of around 7%, thus endorsing the credibility and validity of the forthcoming simulation results to some extent.

4. Results and discussion

4.1. Effect of TEC input current on the cooling performance

Before assessing the thermal behavior of the BTMS, it is necessary to determine an appropriate input current range for the TEC, as a small current can not ensure sufficient cooling effectiveness, while a large current may fail to provide a cooling capacity. Therefore, numerical simulations for a single TEC are conducted under different input currents (I) and temperature conditions, where the temperature difference is set to vary from 0 K to 20 K every 5 K at a fixed cold-side temperature of 300 K. Fig. 4 shows simulation results of the TEC at a temperature difference of 0 K and $I = 5$ A. Detailed boundary conditions for a single TEC are depicted in Fig. 4(a). Driven by the current, holes of p-type thermoelectric semiconductors (shown as red in the picture) and electrons of n-type thermoelectric semiconductors (shown as blue in the picture) will move from the bottom to the top, and then the top side will release heat due to the accumulation of carriers, while the bottom side will absorb heat. On this basis, the TEC can be used as a cooler to control the temperature of electronics. Fig. 4(b) shows the temperature distribution of the TEC. It is observable that even with a temperature difference of 0 K on both sides, the temperature exhibits a variation from 298.53 K to 325.85 K due to the generation of Peltier heat, Joule heat, and Thomson heat. Fig. 4(c) and (d) present the voltage distribution and current density distribution of the TEC, respectively. Along the current direction, the electric potential of the TEC continuously increases with the series connection of thermoelectric semiconductors.

Fig. 5 indicates the cooling performance of the TEC at different input currents and temperature differences. As the input current increases, the cooling power first increases and then decreases, and reaches its maximum value when $I = 5$ A, as shown in Fig. 5(a). According to Eq. (11), when the input current remains at a low level, the Peltier heat dominates, causing the TEC cooling power to increase with the increase

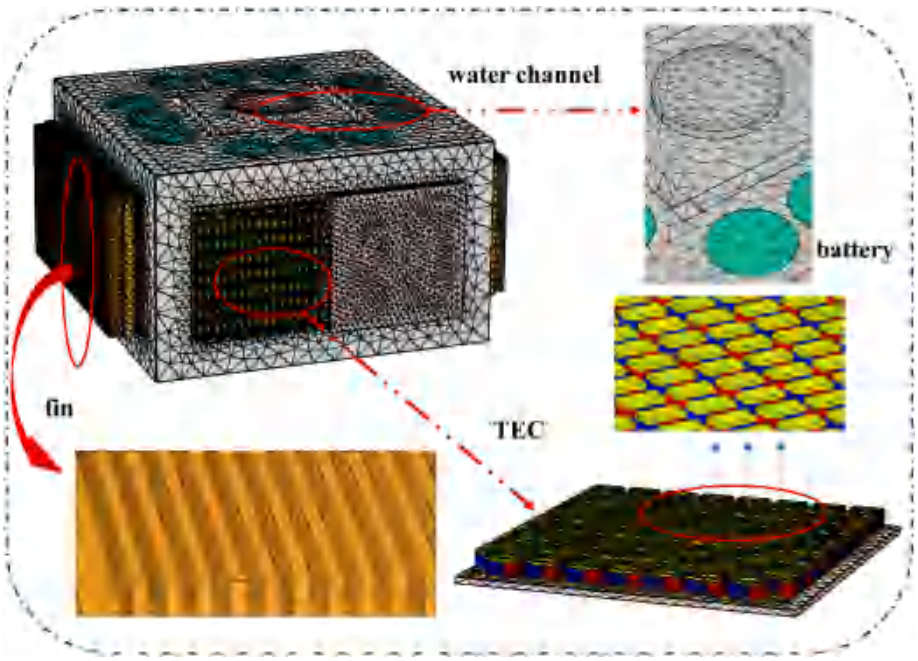

Fig. 2. Details of grid II for the BTMS.

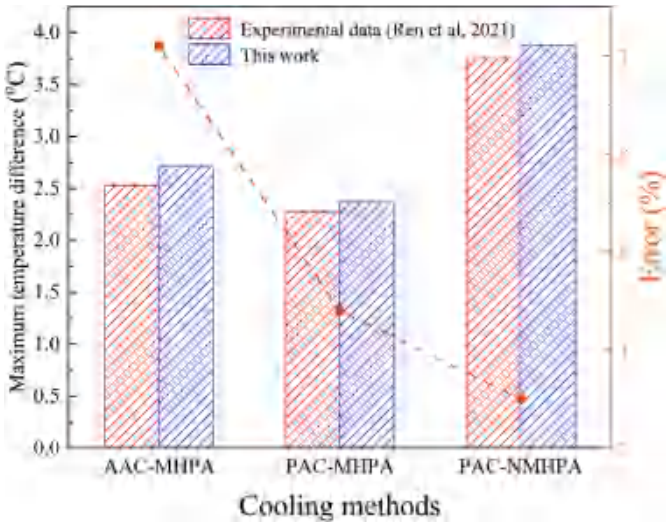

Fig. 3. Comparison of the maximum temperature difference between numerical results and experimental results. (Note: AAC for active air cooling, PAC for passive air cooling, MHPA for micro heat pipe array, and NMHPA for none MHPA).

in current. However, when the current reaches a relatively high level, the Joule heat rapidly increases, leading to a decrease in TEC cooling power with the further increase in current. When the current approaches 5 A, the cooling power reaches its maximum. It is worth noting that for TECs with different thermoelectric parameters, the optimal current varies. Also, cooling power decreases with the increase in temperature difference since the TEC needs to overcome its thermal resistance to provide cooling power. This phenomenon can also explain the corresponding changes in COP in Fig. 5(b). Differently, when the input current is relatively small, the COP can reach a relatively high value, especially when the temperature difference is lower than 10 K. Although the cooling power of the TEC may reach its maximum at 5 A, its COP may be relatively small. Considering both cooling power and COP, an input current range of 1–5 A is suggested, and the influence of input current on the thermal behavior of the BTMS is comprehensively investigated in the following sections.

4.2. Temperature distributions of the BTMS at different TEC input currents

Fig. 6 gives the temperature distribution of the BTMS at $I = 1$ A, 3 A, and 5 A. Here, the air convection heat transfer coefficient and flow speed of cooling water are set as 90 W m^{-2} K^{-1} and 0.11 m s^{-1}, respectively. When $I = 1$ A, 3 A, and 5 A, the maximum temperatures of batteries are 309.89 K, 307.12 K, and 304.69 K, respectively. Compared with a traditional BTMS, in the proposed novel thermoelectric-based BTMS, TECs are used between batteries and cooling devices to further improve the cooling performance of water cooling and air cooling. It can be observed that the temperature of the water channel in the center of the BTMS is lower than that of the heat sink around the BTMS. In general, water cooling outperforms air cooling in reducing the battery temperature, and thus, 4 TECs are arranged on the water channel, while 8 TECs are arranged on the heat sink, to balance the difference in heat dissipation ability between water cooling and air cooling. Consequently, the maximum temperature and temperature difference of batteries could be effectively decreased by increasing the TEC input current.

4.3. Influence of air cooling and TEC input current on the cooling performance of the system

Improving the air convection heat transfer coefficient is able to effectively enhance the cooling performance of heat sinks, but as it further increases, the required energy consumption is higher and the benefits are decreasing. In this case, the use of TECs can address the issue of weakened refrigeration performance and high energy consumption under high heat transfer coefficient conditions with air cooling. Therefore, the influence of air convection heat transfer coefficient on the TEC performance is comprehensively investigated, as shown in Fig. 7. Similarly, as the TEC input current increases, the cooling power (Q_C) of the TEC increases (Fig. 7(a)), while the COP decreases (Fig. 7(b)). Besides, a higher convection heat transfer coefficient is conducive to improving the Q_C and COP, because the heat accumulated on the hot side of the TEC is effectively dissipated by heat sinks with a higher h_{air},

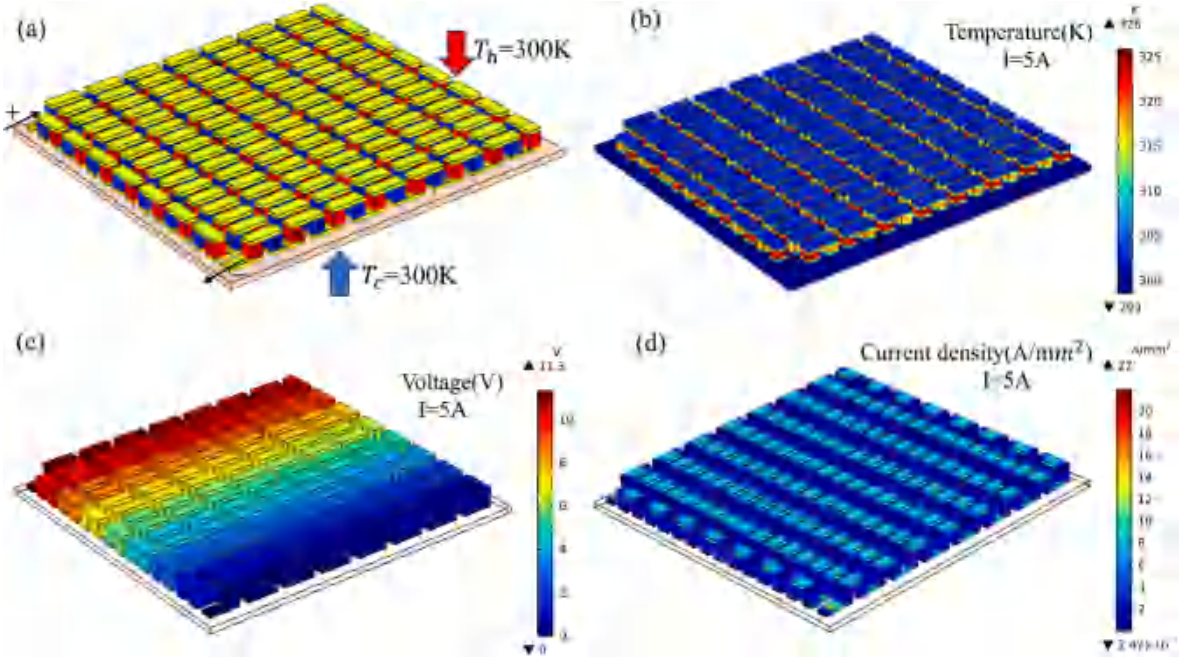

Fig. 4. Numerical simulation results of a single TEC at a temperature difference of 0 K and an input current of 5 A. (a) Finite element model; (b) Temperature distribution; (c) Voltage distribution; (d) Current density distribution.

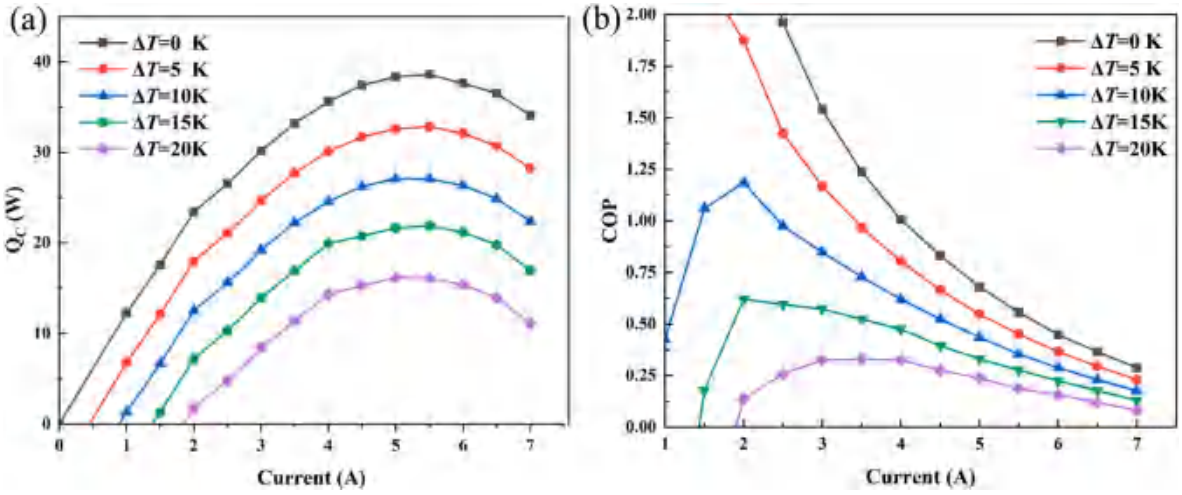

Fig. 5. Cooling performance of the TEC at different input currents and temperature differences. (a) Cooling power Q_C; (b) COP.

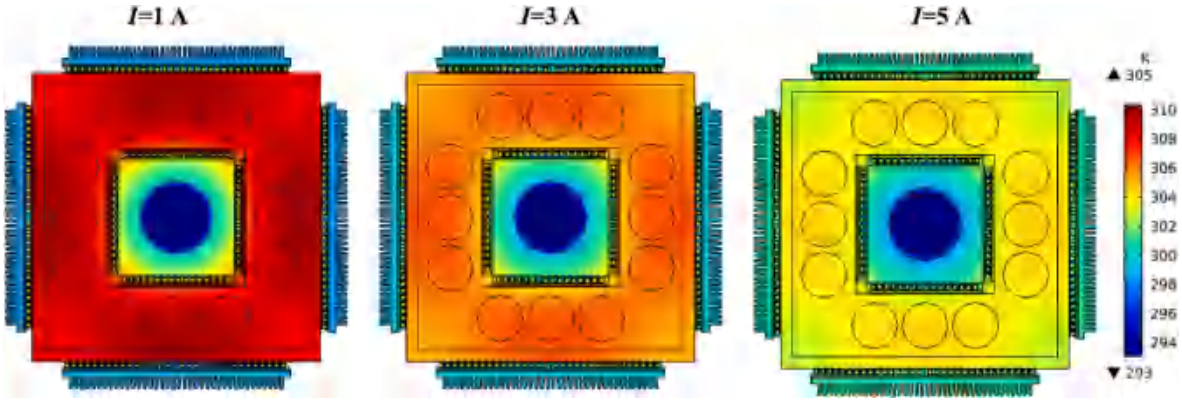

Fig. 6. Temperature distribution characteristics of the BTMS at $I = 1$ A, 3 A, and 5 A.

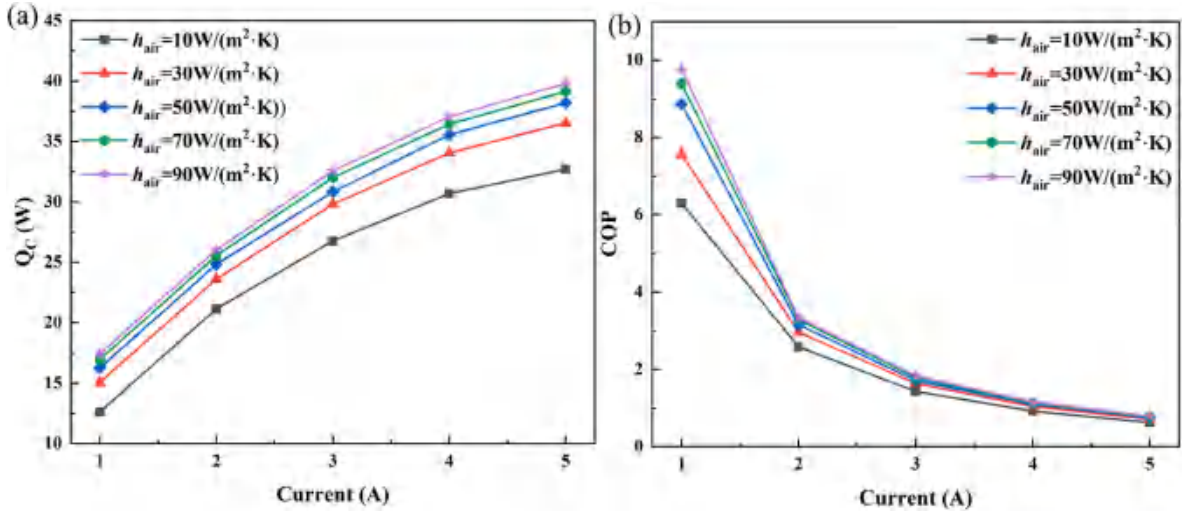

Fig. 7. The effect of air convection heat transfer coefficient on the TEC cooling performance.

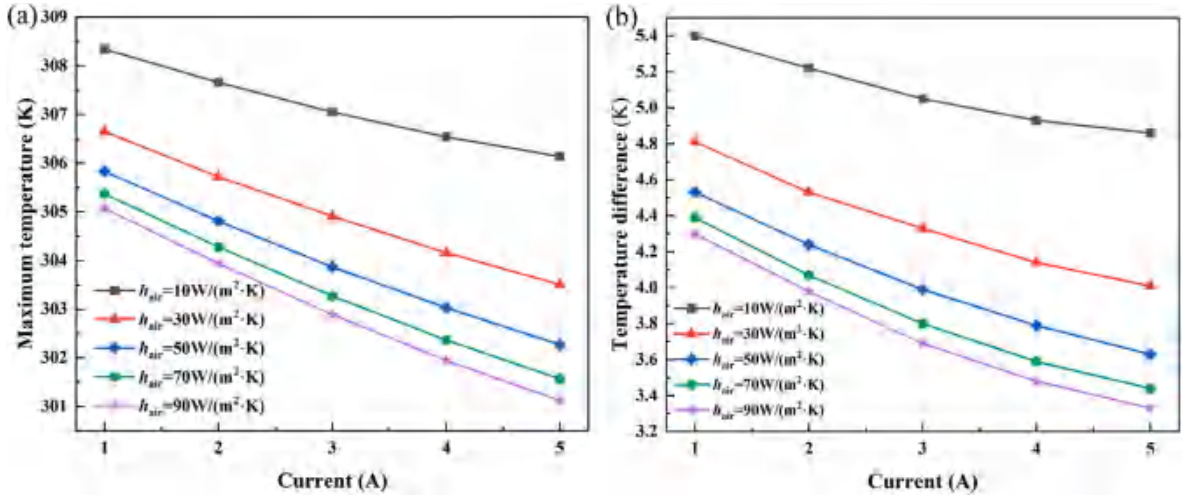

Fig. 8. Maximum temperature and temperature difference of batteries as a function of current at different air convection heat transfer coefficients. (a) Maximum temperature; (b) Temperature difference.

and the temperature difference on both sides of the TEC decreases. According to Fig. 5, a lower temperature difference is beneficial to improve the TEC cooling performance. However, when h_{air} reaches a relatively high value, its impact on TEC cooling performance weakens. Considering the large energy consumption and low benefits of cooling performance improvement, the convection heat transfer coefficient is suggested to be lower than 50 W m^{-2} K^{-1}. Accordingly, when h_{air} is higher than 50 W m^{-2} K^{-1}, it is not recommended to further improve air cooling performance instead of using a higher TEC input current.

Fig. 8 shows the maximum temperature and temperature difference of batteries as a function of current at different air convection heat transfer coefficients. When the TEC input current increases, both the maximum temperature and temperature difference of batteries decrease, because of the increased cooling power produced by TECs. Also, an increase in the air convection heat transfer coefficient is helpful to improve the thermal performance of batteries. On the one hand, the increase in h_{air} can directly lower the temperature of the whole BTMS. On the other hand, the temperature difference on both sides of TECs also decreases, thereby enhancing the cooling performance of the TEC. Compared with the BTMS at h_{air} = 10 W m^{-2} K^{-1} and I = 1 A, its maximum temperature and temperature difference at h_{air} = 90 W m^{-2} K^{-1} and I = 5 A are decreased by 2.34% and 38.33%, respectively. However, with the increase of air convection heat transfer coefficient, the improvement of BTMS cooling performance gradually weakens, as shown in Fig. 9, while at the same time, accompanied by a significant increase in energy consumption. When h_{air} is higher than 50 W m^{-2} K^{-1}, the effect on the temperature of the entire BTMS is insignificant, and as h_{air} increases from 50 W m^{-2} K^{-1} to 90 W m^{-2} K^{-1}, the temperature of the BTMS only decreases slightly. Therefore, the combination of air cooling and TECs can effectively reduce the maximum temperature and temperature difference of batteries. At the same time, the use of TEC in the battery system can reduce the dependence on air cooling, and the air convection heat transfer coefficient of below 50 W m^{-2} K^{-1} already meets the requirements, thereby reducing the energy consumption of the heat sink.

Fig. 10 illustrates temperature distributions (xz-axis cross-section) of a single cell at different air convection heat transfer coefficients, with a TEC input current of 1 A and a water flow speed of 0.11 m/s. The left side of the battery cross-section is close to the outer 8 TECs, while the right side is close to the inner 4 TECs. When h_{air} = 90 W m^{-2} K^{-1}, the battery temperature on the left side is obviously higher than that on the right side. This is attributed to the fact that water cooling outperforms air cooling at this time, and the temperature difference between the two ends of the internal TEC is lower than that of the external TEC, thus

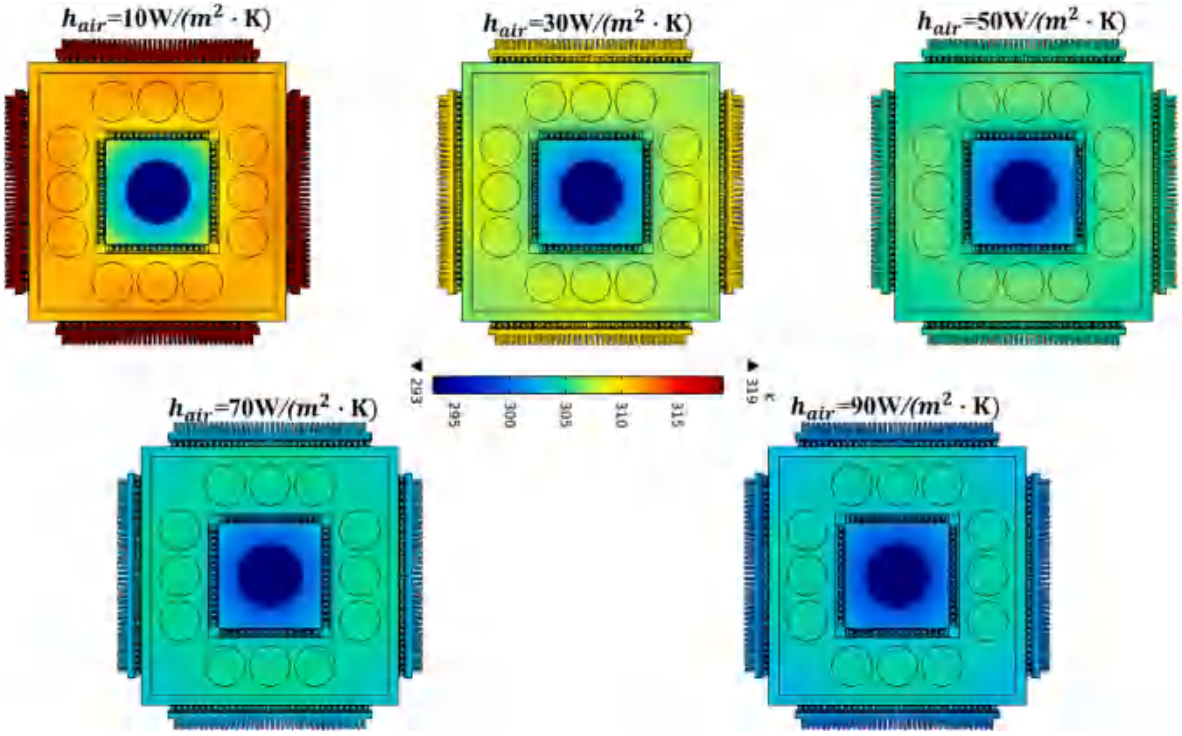

Fig. 9. Temperature distributions throughout the structure of the BTMS at different air convection heat transfer coefficients.

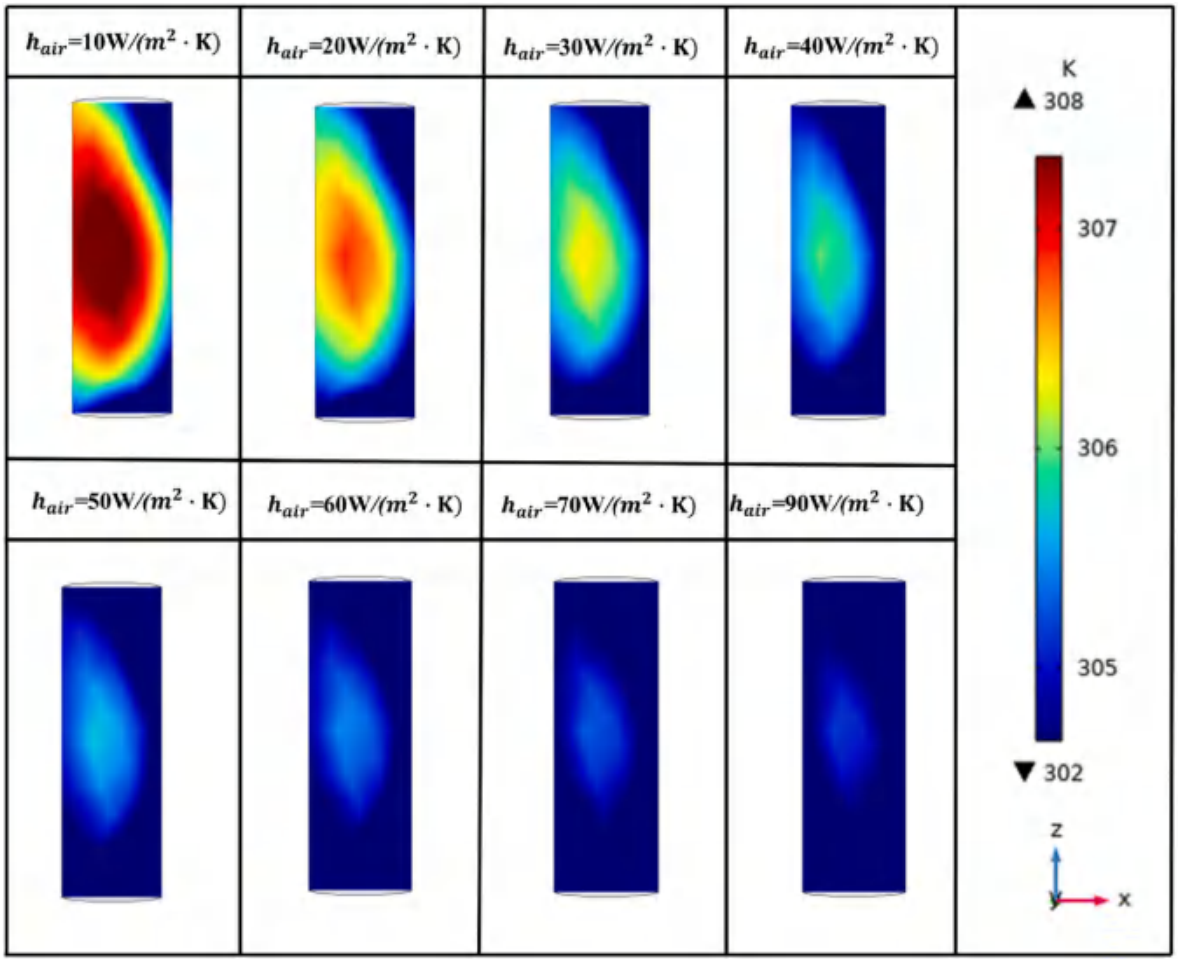

Fig. 10. Temperature distributions of a single battery cell in the xz-axis cross-section.

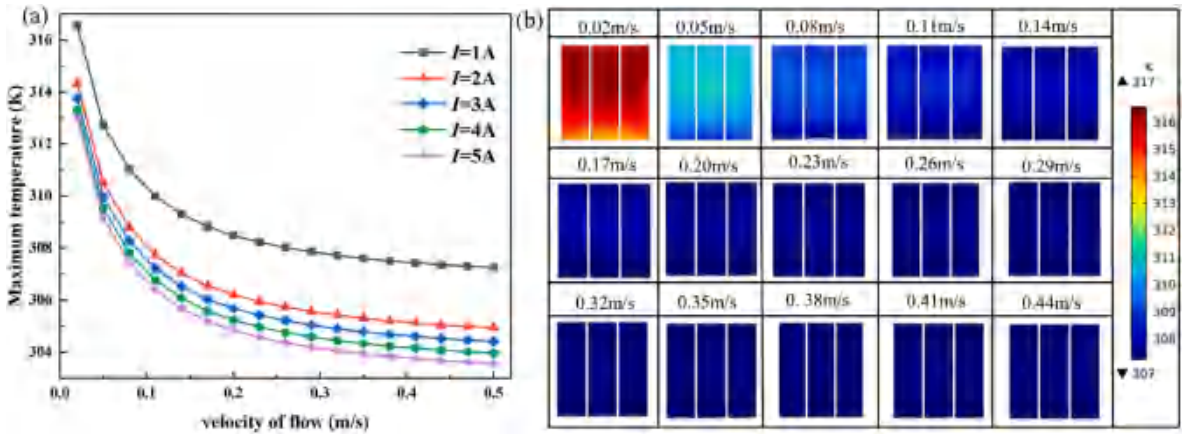

Fig. 11. Effect of different flow speeds of cooling water on the thermal performance of the BTMS. (a) Effect of water flow speed on the maximum temperature of batteries; (b) Temperature distributions of batteries at different water flow speeds.

providing a higher cooling power. Additionally, as the air convection heat transfer coefficient increases, the battery temperature on the left side gradually approaches and equals the battery temperature on the right side, because the cooling performance of the outer 8 TECs also improves. This phenomenon highlights the advantages of the proposed thermoelectric-based BTMS in minimizing the temperature difference of batteries.

4.4. Influence of water cooling and TEC input current on the cooling performance of the system

Similarly, the flow speed of cooling water has a significant influence on the cooling performance of the internal 4 TECs. Fig. 11 shows the effect of different flow speeds of cooling water on the thermal performance of the BTMS. Here, the air convection heat transfer coefficient is fixed at 50 W m^{-2} K^{-1} according to the above analysis. According to Fig. 11(a), the maximum temperature of batteries decreases with the increase in water flow speed, especially when the water flow speed is at a relatively low value. With a further increase in water flow speed, its influence on the maximum temperature diminishes, which is consistent with the trend of air convection heat transfer coefficient in Fig. 8. In addition, the greater the TEC input current is, the lower the maximum temperature of batteries will be. Detailed temperature distributions of batteries at different water flow speeds are presented in Fig. 11(b),

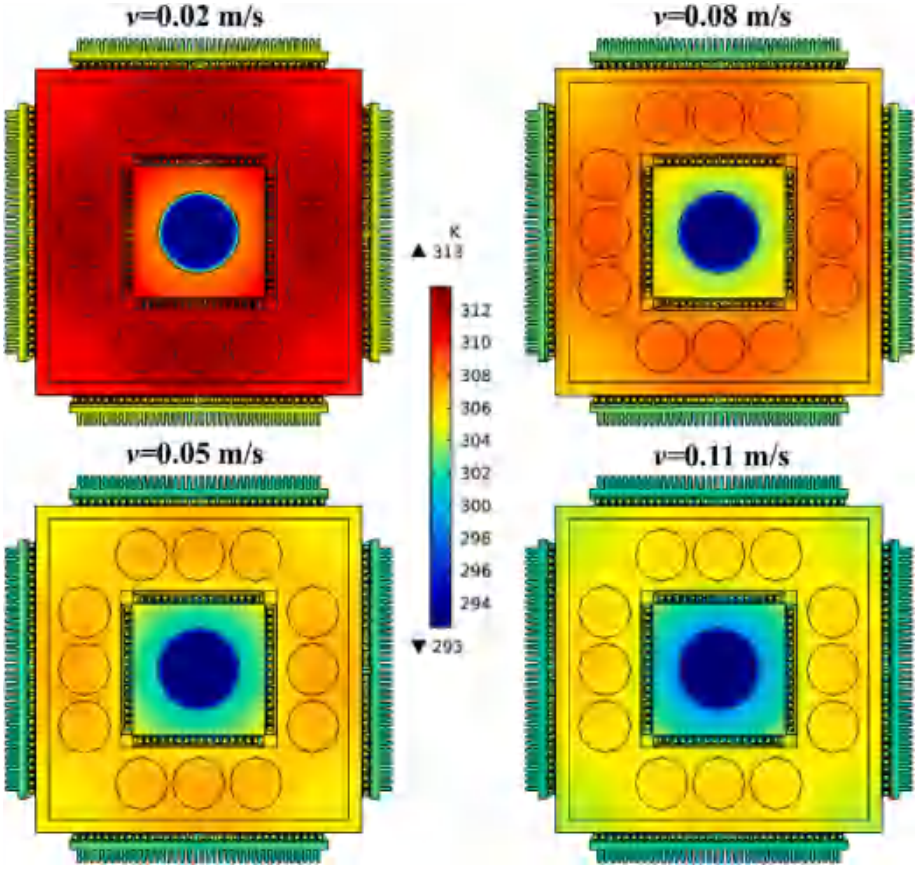

Fig. 12. Temperature distributions of the entire BTMS at different water flow speeds from 0.02 m/s to 0.11 m/s.

where the TEC input current is set to be 1 A. As can be observed, when the water flow speed is larger than 0.11 m/s, the changes have negligible impact on the maximum temperature and temperature difference of batteries. When the water flow speed is lower than 0.11 m/s, a minimum flow rate limitation needs to be determined.

Fig. 12 shows temperature distributions of the entire BTMS at different water flow speeds from 0.02 m/s to 0.11 m/s. It is evident that for a water flow speed of 0.02 m/s, the maximum battery temperature of 313 K may exceed the optimal temperature range of lithium-ion batteries (from 273 K to 313 K). Therefore, a water flow speed range from 0.02 m/s to 0.11 m/s is suggested for the given thermoelectric-based BTMS. However, only the minimum TEC input current of 1 A and the medium air convection heat transfer coefficient of 50 W m^{-2} K^{-1} are used herein to explore the optimal water flow speed. The fluctuations of the TEC input current and air convection heat transfer coefficient may result in a different optimal range of water flow speed.

Fig. 13 shows the maximum temperature and temperature difference of batteries under different working conditions. Here, two extreme air convection heat transfer coefficients of 10 and 90 W m^{-2} K^{-1} are selected to analyze its sensitivity to water cooling parameters. At a TEC input current of 1 A and h_{air} = 90 W m^{-2} K^{-1}, the maximum temperatures for cooling water free, flow speed of 0.02 m/s and 0.11 m/s are 335.51 K, 311.28 K, and 304.88 K, respectively, as shown in Fig. 13(a). Consequently, water cooling is indispensable for reducing battery temperature, even if the air cooling and TEC cooling reach the maximum level. Besides, at a water flow speed of 0.11 m/s, the temperature difference of batteries is significantly lower than that observed at a flow rate of 0.02 m/s, as shown in Fig. 13(b). However, in the situation of water cooling free, the temperature difference decreases first and then increases as the increase of TEC input current. This phenomenon occurs because, at lower TEC input currents, the cooling power increases proportionally with the current. Nevertheless, when the current is further increased, the generated heat on the hot side of TECs can not be dissipated by cooling water, resulting in a degradation of the cooling performance and a decrease in the temperature difference.

Fig. 13(c) shows the corresponding maximum temperature of batteries at h_{air} = 10 W m^{-2} K^{-1}. It seems that as the TEC input current increases, the maximum temperature only maintains a small change. Under the conditions of minimum cooling input of h_{air} = 10 W m^{-2} K^{-1}, TEC input current of 1 A, and water flow speed of 0.02 m/s, the maximum temperature reaches 319.14 K, exceeding the optimal temperature of 313 K, but when the water flow speed is increased to 0.11 m/s, the maximum temperature drops to 308.06 K. Regarding the temperature difference of batteries, the variation trend in Fig. 13(d) aligns with that in Fig. 13(b), but when the water flow speed is 0.02 m/s, the temperature difference has already exceeded the optimal value of 5 K, whereas 0.11 m/s meets the requirement.

Above all, a certain range of air cooling and water cooling is crucial to ensure the optimal operating temperature of the proposed BTMS. Considering the low influence on cooling performance and high energy consumption, it is not recommended to set excessively high air convection heat transfer coefficients and water flow speed, instead, ranges of h_{air} = 10 W m^{-2} K^{-1} to 50 W m^{-2} K^{-1} and 0.02 m/s to 0.11 m/s are suggested. Under the minimum cooling input (10 W m^{-2} K^{-1}, 0.02 m/s,

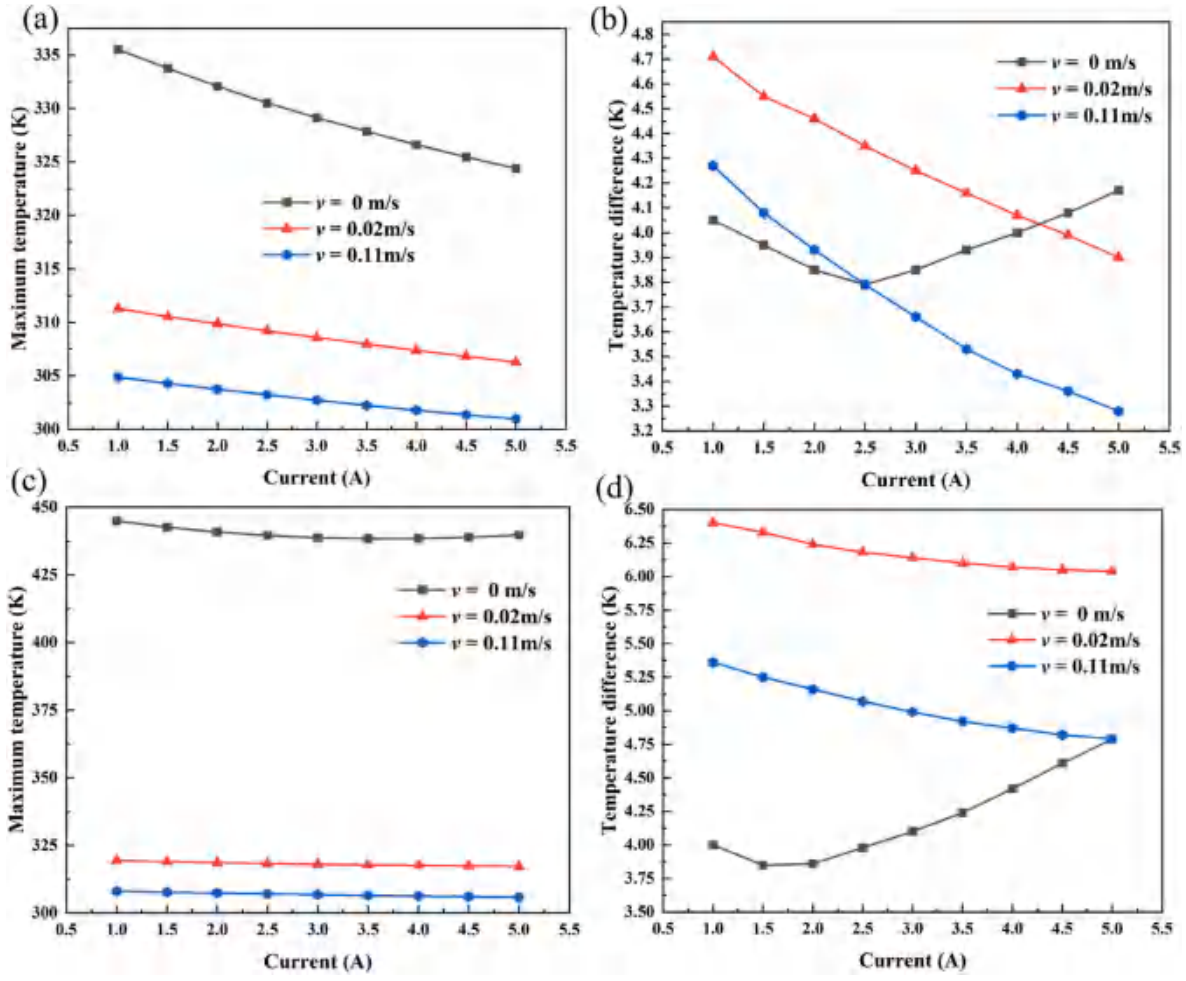

Fig. 13. Effects of different working conditions on the maximum temperature and temperature difference of the battery. (a) Maximum temperature at h_{air} = 90 W m^{-2} K^{-1}; (b) Temperature difference at h_{air} = 90 W m^{-2} K^{-1}; (c) Maximum temperature at h_{air} = 10 W m^{-2} K^{-1}; (d) Temperature difference at h_{air} = 10 W m^{-2} K^{-1}.

and 1A), the maximum temperature and temperature difference of batteries are 319.14 K and 6.40 K respectively, slightly exceeding the optimal operating temperatures of lithium-ion batteries (maximum temperature of 313 K [37] and temperature difference of 5 K [7]), while those decrease to 302.27 K and 3.63 K respectively under the maximum cooling input (50 W m^{-2} K^{-1}, 0.11 m/s, and 5 A). In real applications, precise control of battery temperature can be achieved by adjusting the air cooling, water cooling, and TEC input current. At the same time, energy consumption should be considered to ultimately determine the corresponding inputs of different cooling parameters.

5. Conclusions

In the present work, a novel thermoelectric-based BTMS coupled with water cooling and air cooling is proposed to improve the thermal behavior of batteries. Besides, a hydraulic-thermal-electric multiphysics model for the BTMS is established to assess its behavior under different cooling parameters, including TEC input current, air convection heat transfer coefficient, and flow speed of cooling water. According to the numerical results, the key findings can be summarized as follows:

(1) The introduction of TECs into the BTMS can effectively improve the thermal behavior of batteries. Both the maximum temperature and temperature difference of batteries significantly decrease with the increase of TEC input current. The cooling performance of TECs first increases and then decreases with the increase of input current, reaching its maximum value when the current is 5 A. Additionally, the temperature difference across the TEC adversely affects its cooling performance.
(2) The maximum temperature and temperature difference of batteries decrease with an increase in air convection heat transfer coefficient, and the use of TECs between the heat sink and batteries can further amplify the cooling effect of air cooling. However, when the air convection heat transfer coefficient exceeds 50 W m^{-2} K^{-1}, its impact on the thermal performance of the BTMS weakens, while the energy consumption increases.
(3) The battery temperature exhibits a decrease as the water flow rate increases, indicating that higher water flow rates improve the cooling performance of the TEC. However, the rate of temperature reduction diminishes as the flow rates continue to rise. Moreover, water cooling is crucial for reducing the battery temperature since even a relatively small flow rate of cooling water can significantly improve the cooling ability of TECs by reducing their thermal resistance, thereby improving the thermal performance of the BTMS
(4) Herein, the ranges of 10 W m^{-2} K^{-1} to 50 W m^{-2} K^{-1}, 0.02 m/s to 0.11 m/s, and 1 A to 5A are suggested for air cooling, water cooling, and TEC input current, respectively. To ensure optimal performance of the proposed BTMS, the cooling parameters of 50 W m^{-2} K^{-1}, 0.11 m/s, and 5 A are suggested, corresponding to the maximum temperature and temperature difference of 302.27 K and 3.63 K, respectively. However, the cooling parameters of these three factors interact with each other. If they are all at their minimum values, the battery temperature will slightly exceed the optimal value. Therefore, it is vital to select appropriate cooling parameters within these ranges to balance the thermal performance and energy consumption of the BTMS.
(5) It is essential to develop appropriate control strategies to simultaneously adjust the parameters of TEC input current, air cooling, and water cooling, in order to improve the thermal performance of the BTMS while reducing energy consumption. However, this control strategy is complicated and will be studied in future works.

CRediT authorship contribution statement

Ding Luo: Conceptualization, Methodology, Resources, Writing – original draft. **Ye Zhao:** Data curation, Validation, Visualization. **Jin Cao:** Software. **Wei-Hsin Chen:** Writing – review & editing. **Yulong Zhao:** Formal analysis. **Bingyang Cao:** Project administration, Supervision, Writing – review & editing.

Declaration of competing interest

We declare that we do not have any commercial or associative interest that represents a conflict of interest in connection with the work submitted.

Acknowledgments

This work was supported by the National Natural Science Foundation of China (Grant Nos. 52306017, U20A20301, 52250273), and the Natural Science Foundation of Hubei Province (No. 2023AFB093).

References

[1] W He, Q Xu, S Liu, T Wang, F Wang, X Wu, et al., Analysis on data center power supply system based on multiple renewable power configurations and multi-objective optimization, Renewable Energy 222 (2024) 119865.
[2] Y Zhao, W Li, X Zhao, Y Wang, D Luo, Y Li, et al., Energy and exergy analysis of a thermoelectric generator system for automotive exhaust waste heat recovery, Appl Therm Eng 239 (2024) 122180.
[3] D. Luo, H. Wu, J. Cao, Y. Yan, X. Yang, B. Cao, Numerical investigation of a battery thermal management system integrated with vapor chamber and thermoelectric refrigeration, J. Clean. Prod. 434 (2024) 140089.
[4] K.G. Logan, J.D. Nelson, X. Lu, A. Hastings, UK and China: will electric vehicle integration meet Paris Agreement Targets? Transp. Res. Interdiscip. Perspect. 8 (2020).
[5] D. Luo, Z. Wu, Y. Yan, J. Cao, X. Yang, Y. Zhao, et al., Performance investigation and design optimization of a battery thermal management system with thermoelectric coolers and phase change materials, J. Clean. Prod. 434 (2024) 139834.
[6] E. Mossali, N. Picone, L. Gentilini, O. Rodriguez, J.M. Perez, M. Colledani, Lithium-ion batteries towards circular economy: a literature review of opportunities and issues of recycling treatments, J. Environ. Manag. 264 (2020) 110500.
[7] Y. Gan, L. He, J. Liang, M. Tan, T. Xiong, Y. Li, A numerical study on the performance of a thermal management system for a battery pack with cylindrical cells based on heat pipes, Appl. Therm. Eng. (2020) 179.
[8] K. Kirad, M. Chaudhari, Design of cell spacing in lithium-ion battery module for improvement in cooling performance of the battery thermal management system, J. Power Sources (2021) 481.
[9] Y. Fan, Y. Bao, C. Ling, Y. Chu, X. Tan, S. Yang, Experimental study on the thermal management performance of air cooling for high energy density cylindrical lithium-ion batteries, Appl. Therm. Eng. 155 (2019) 96–109.
[10] W. Li, M. Xiao, X. Peng, A. Garg, L. Gao, A surrogate thermal modeling and parametric optimization of battery pack with air cooling for EVs, Appl. Therm. Eng. 147 (2019) 90–100.
[11] C. Menale, F. D'Annibale, B. Mazzarotta, R. Bubbico, Thermal management of lithium-ion batteries: an experimental investigation, Energy 182 (2019) 57–71.
[12] H. Zhou, F. Zhou, Q. Zhang, Q. Wang, Z. Song, Thermal management of cylindrical lithium-ion battery based on a liquid cooling method with half-helical duct, Appl. Therm. Eng. (2019) 162.
[13] S. Panchal, R. Khasow, I. Dincer, M. Agelin-Chaab, R. Fraser, M. Fowler, Thermal design and simulation of mini-channel cold plate for water cooled large sized prismatic lithium-ion battery, Appl. Therm. Eng. 122 (2017) 80–90.
[14] J. Du, Y. Sun, Y. Huang, X. Wu, Analysis of influencing factors of thermal management system for LiFePO4 lithium battery under high power charging, World Electric Vehicle Journal 11 (2020).
[15] U. Chavan, O. Prajapati, P. Hujare, Lithium ion battery thermal management by using coupled heat pipe and liquid cold plate, Mater. Today: Proc. 80 (2023) 382–388.
[16] R. Ren, Y. Zhao, Y. Diao, L. Liang, H. Jing, Active air cooling thermal management system based on U-shaped micro heat pipe array for lithium-ion battery, J. Power Sources (2021) 507.
[17] Z. Ling, F. Wang, X. Fang, X. Gao, Z. Zhang, A hybrid thermal management system for lithium ion batteries combining phase change materials with forced-air cooling, Appl. Energy 148 (2015) 403–409.
[18] M.M. Farid, A.M. Khudhair, S.A.K. Razack, S. Al-Hallaj, A review on phase change energy storage: materials and applications, Energy Convers. Manag. 45 (2004) 1597–1615.
[19] W.Q. Li, Z.G. Qu, Y.L. He, Y.B. Tao, Experimental study of a passive thermal management system for high-powered lithium ion batteries using porous metal foam saturated with phase change materials, J. Power Sources 255 (2014) 9–15.

[20] Z.G. Qu, W.Q. Li, W.Q. Tao, Numerical model of the passive thermal management system for high-power lithium ion battery by using porous metal foam saturated with phase change material, Int. J. Hydrogen Energy 39 (2014) 3904–3913.
[21] W.H. Zhu, H. Yang, K. Webb, T. Barron, P. Dimick, B.J. Tatarchuk, A novel cooling structure with a matrix block of microfibrous media/phase change materials for heat transfer enhancement in high power Li-ion battery packs, J. Clean. Prod. 210 (2019) 542–551.
[22] A. Babapoor, M. Azizi, G. Karimi, Thermal management of a Li-ion battery using carbon fiber-PCM composites, Appl. Therm. Eng. 82 (2015) 281–290.
[23] F. Samimi, A. Babapoor, M. Azizi, G. Karimi, Thermal management analysis of a Li-ion battery cell using phase change material loaded with carbon fibers, Energy 96 (2016) 355–371.
[24] P. Goli, S. Legedza, A. Dhar, R. Salgado, J. Renteria, A.A. Balandin, Graphene-enhanced hybrid phase change materials for thermal management of Li-ion batteries, J. Power Sources 248 (2014) 37–43.
[25] J. Weng, Y. He, D. Ouyang, X. Yang, G. Zhang, J. Wang, Thermal Performance of PCM and Branch-Structured Fins for Cylindrical Power Battery in a High-Temperature Environment, vol. 200, Energy Conversion and Management, 2019.
[26] M. Hao, J. Li, S. Park, S. Moura, C. Dames, Efficient thermal management of Li-ion batteries with a passive interfacial thermal regulator based on a shape memory alloy, Nat. Energy 3 (2018) 899–906.
[27] W. Song, F. Bai, M. Chen, S. Lin, Z. Feng, Y. Li, Thermal management of standby battery for outdoor base station based on the semiconductor thermoelectric device and phase change materials, Appl. Therm. Eng. 137 (2018) 203–217.
[28] X. Liu, C.-F. Zhang, J.-G. Zhou, X. Xiong, Y.-P. Wang, Thermal performance of battery thermal management system using fins to enhance the combination of thermoelectric Cooler and phase change Material, Appl. Energy (2022) 322.
[29] Q. Hu, D. Luo, J. Guo, W. Qiu, X. Wu, L. Yang, et al., Broad temperature plateau for high thermoelectric properties of n-type Bi(2)Te(2.7)Se(0.3) by 3D printing-driven defect engineering, ACS Appl. Mater. Interfaces 15 (2023) 1296–1304.
[30] T. Ma, X. Lu, J. Pandit, S.V. Ekkad, S.T. Huxtable, S. Deshpande, et al., Numerical study on thermoelectric–hydraulic performance of a thermoelectric power generator with a plate-fin heat exchanger with longitudinal vortex generators, Appl. Energy 185 (2017) 1343–1354.
[31] H. Pang, L. Wu, J. Liu, X. Liu, K. Liu, Physics-informed neural network approach for heat generation rate estimation of lithium-ion battery under various driving conditions, J. Energy Chem. 78 (2023) 1–12.
[32] D. Luo, Y. Yan, W.-H. Chen, X. Yang, H. Chen, B. Cao, et al., A comprehensive hybrid transient CFD-thermal resistance model for automobile thermoelectric generators, Int. J. Heat Mass Tran. 211 (2023) 124203.
[33] D. Luo, Y. Li, Y. Yan, X. Hu, Xa Fan, W.-H. Chen, et al., Realizing ultrahigh ZT value and efficiency of the Bi2Te3 thermoelectric module by periodic heating, Energy Convers. Manag. 296 (2023) 117669.
[34] C.M. Hamisi, G.B. Gerutu, K.A. Greyson, P.V. Chombo, Thermal behavior of lithium-ion battery under variation of convective heat transfer coefficients, surrounding temperatures, and charging currents, J. Loss Prev. Process. Ind. (2022) 80.
[35] L.A. Nimmagadda, R. Mahmud, S. Sinha, Materials and devices for on-chip and off-chip peltier cooling: a review, IEEE Trans. Compon. Packag. Manuf. Technol. 11 (2021) 1267–1281.
[36] R. Ren, Y. Zhao, Y. Diao, L. Liang, H. Jing, Active air cooling thermal management system based on U-shaped micro heat pipe array for lithium-ion battery, J. Power Sources 507 (2021) 230314.
[37] Z.Y. Jiang, H.B. Li, Z.G. Qu, J.F. Zhang, Recent progress in lithium-ion battery thermal management for a wide range of temperature and abuse conditions, Int. J. Hydrogen Energy 47 (2022) 9428–9459.